Case Studies in Thermal Engineering 65 (2025) 105684

Contents lists available at ScienceDirect

Case Studies in Thermal Engineering

journal homepage: www.elsevier.com/locate/csite

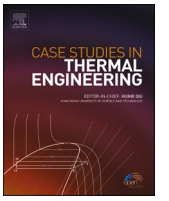

Numerical investigation on heat transfer and flow mechanism in microchannel heat sink having V shape ribs

Naushad Ali [a], Injamamul Haque [a], Tabish Alam [b,*], Tauseef Uddin Siddiqui [c], Mushtaq Ahmad Ansari [d], Jagmohan Yadav [a], Shivam Srivastava [a], Erdem Cuce [e,f,g,h], Intesaaf Ashraf [i], Dan Dobrotă [j]

[a] Department of Mechanical Engineering, Mahatma Jyotiba Phule Rohilkhand University, Bareilly, 243006, India
[b] Architecture, Planning & Energy Efficiency, CSIR-Central Building Research Institute, Roorkee, 247667, Uttarakhand, India
[c] Mechanical Engineering Department, Jamia Millia Islamia, Jamia Nagar, Okhla, New Delhi, Delhi, 110025, India
[d] Department of Pharmacology and Toxicology, College of Pharmacy, King Saud University, Riyadh, 11451, Saudi Arabia
[e] Department of Mechanical Engineering, Faculty of Engineering and Architecture, Recep Tayyip Erdogan University, Zihni Derin Campus, 53100, Rize, Turkey
[f] Center for Research Impact & Outcome, Chitkara University, Rajpura, 140401, Punjab, India
[g] University Centre for Research and Development, Chandigarh University, Mohali, Punjab, 140413, India
[h] Department of Mechanical Engineering, Saveetha School of Engineering, Saveetha Institute of Medical and Technical Sciences, Saveetha University, Chennai, India
[i] Mechanical Engineering Department, UCL, London, WC1E, United Kingdom
[j] Faculty of Engineering, Department of Industrial Engineering and Management, Lucian Blaga University of Sibiu, 550024, Sibiu, Romania

ARTICLE INFO

Keywords:
Microchannel heat sink
Vortex generator
Heat transfer enhancement
CFD simulation
Coolant fluid

ABSTRACT

This research comprehensively examines the influence of the V-shaped rib angle of attack on the thermal and hydraulic efficacy of microchannel heat sinks (MCHS), employing Computational Fluid Dynamics (CFD) simulations over Reynolds numbers ranging from 100 to 900. The primary innovation of this investigation resides in the methodical analysis of the impacts of varying rib angles, specifically from 35° to 90°, on both heat transfer and flow resistance within the MCHS framework. The findings indicate that a reduced angle of attack, notably 35°, markedly improves thermal performance, as evidenced by the Nusselt number (*Nu*) achieving a value of 13.81 at a Reynolds number of 300, in contrast to a mere 8.12 at 90°. This enhancement in thermal transfer is ascribed to the more effective turbulence produced at lower angles, which optimizes convective heat transfer while minimizing excessive resistance. Importantly, this study also underscores the dual effect of rib angle on flow dynamics, as diminished angles elevate friction factor (f), necessitating increased energy input for fluid movement—friction factor at a Reynolds number of 300 were recorded at 0.0465 for 35° and 0.0288 for 90°, thereby validating the compromise between heat transfer and flow resistance. This research offers a novel perspective that while elevated rib angles (approaching 90°) mitigate hydraulic resistance, they concurrently reduce the enhancement of heat transfer, thereby accentuating the necessity for an optimized rib angle to achieve equilibrium between thermal and hydraulic performance.

* Corresponding author.
E-mail address: tabish.iitr@gmail.com (T. Alam).

https://doi.org/10.1016/j.csite.2024.105684
Received 5 October 2024; Received in revised form 1 December 2024; Accepted 20 December 2024
Available online 22 December 2024

Nomenclature

		$\overline{h}$	Avg. heat transfer coefficient, $W.m^{-2}.K^{-1}$
A	Area, m^2	q	Constant heat flux, $W.m^{-2}$
A_c	Cooling surface area, m^2		***Greek symbols***
A_q	Heat flux area, m^2	α	Poisson's ratio
C_p	Specific heat, $J.(kg.K)^{-1}$	β	Thermal expansion
D_h	Hydraulic dia of the passage, mm	η	Thermal efficiency
E	Young's modulus, Pa	θ	Attack angle of rib
f/f_s	Friction factor ratio	μ	Dynamic viscosity, Pa.s
H	Height, mm	ρ	Density, $kg.m^{-3}$
H_{ch}	Passage height, mm		***Subscripts***
H_s	MCHS solid bottom height, mm	ch	Channel
k	Thermal conductivity, (W/m.K)	f	Fluid
L	Length, mm	m/mc	Microchannel
Nu_s	Nusselt number of smooth channel	s	Solid
p	Pitch, mm	sw	Side wall
P	Pressure, Pa		***Abbreviations***
ΔP	Pressure drop, Pa	CFD	Computational fluid dynamics
T	Temperature, K	f	Friction factor
T_c	Avg. temperature for conjugated area, K	HTF	Heat Transfer fluid
T_f	Avg. temperature of fluid, K	MCHS	Microchannel heat sink
u_m	Mean velocity of fluid, $m.s^{-1}$	*Nu*	Nusselt number
W	Channel width, mm	PVT	Photovoltaic thermal
W_{ch}	Passage width, mm	Re	Reynolds number
W_{sw}	Channel side wall width, mm	THPP	Thermohydraulic performance parameter

1. Introduction

Microchannel heat sinks (MCHS) have emerged as a revolutionary technology in thermal management due to their high heat dissipation capabilities and compact size. These devices consist of the numerous parallel microchannels, typically with widths and heights in the range of tens to hundreds of the micrometers. Large surface area-to-volume ratio provided by MCHS allows for efficient heat transfer from a heat-generating source to the coolant flowing through channels. MCHS are essentials for cooling high-power electronic devices like CPUs and GPUs, providing superior the thermal performance to prevent overheating and enhance component lifespan [1]. In Photovoltaic Thermal (PVT) collectors, it manages thermal energy, improving electrical and thermal efficiency by maintaining the lower operating temperatures for photovoltaic cells [2]. Beyond electronics and PVT systems, microchannel heat sinks are used in the aerospace, automotive, and biomedical fields, cooling the high-performance engines, power electronics, and medical devices to ensure optimal its functionality and reliability through effective thermal management in large [3–5].

MCHS enhance cooling through increased the surface area and high he thermal conductivity materials in passive cooling, as well as by leveraging forced convection techniques. The microchannels significantly expand the heat transfer surface/area, while materials like copper or silicon ensure with efficient thermal conduction [6]. In forced convection, coolants i.e. heat transfer fluid are actively pumped through the channels, creating high velocity and the turbulent flow that increases the heat transfer coefficient [7]. Optimized the channel designs, such as varying the cross-sectional areas or adding interruptions, further enhance turbulence and heat dissipation [8]. These combined methods make MCHS highly effective for thermal management in high-power and compact applications.

The exploration of microchannels as heat exchangers was pioneered by Tuckerman and Pease in 1981 [9]. whose findings demonstrated that reducing the hydraulic diameter of these channels markedly enhances the heat transfer coefficient relative to traditional heat exchangers. Subsequent investigations delved into the intricacies of heat transfer processes within microchannels and reinforced the validity of continuum theory for incompressible fluid flow [10–12]. Sabbah et al. [13] conducted an in-depth analysis of three-dimensional heat transfer phenomena within microchannel heat sinks, encompassing both solid and liquid phases. Their study affirmed that conventional momentum and energy conservation laws remain applicable, provided that the microchannel width significantly surpasses the mean free path of water molecules.

MCHS typically operate within the laminar flow regime, characterized by low Reynolds numbers (Re) ranging from 100 to 900 [6, 14]. Conventional MCHS configurations feature linear flow passages, resulting in parallel streamlines that lack the capacity for flow mixing. Consequently, the thermal boundary layer's thickness progressively increases along the flow path, thereby imposing greater thermal resistance and diminishing thermal performance [15,16]. To ameliorate this issue and augment the heat dissipation rate of MCHS, it is imperative to induce flow mixing and enhance thermal diffusion within the flow, which can be achieved by employing the passive techniques. Passive techniques are widely recognized as the optimal approach for achieving superior heat dissipation rates while necessitating minimal modifications to geometrical configurations. The significance of passive techniques for enhancing the performance of MCHS is escalating, attributable to their simplicity of implementation. These methodologies encompass modifications to the geometric configurations of flow passages, exemplified by the incorporation of trapezoidal grooves [17], two side wedges [17], wavy channel [18], pin fins of different shapes such as oval shape [17], semi elliptical pin fins [14], airfoil shaped pin fins [19].

A plethora of numerical investigations have been undertaken to elucidate the mechanisms underpinning heat transfer, and various enhancements have been proposed to augment heat transfer efficacy. Previous investigations have employed an array of rib configurations to augment heat transfer by inducing turbulence within fluid dynamics. Illustrative examples encompass triangular wing vortex generators [20], inclined punched ribs and grooves [21], multiple V-shaped ribs [22], spanwise V-ribs (multiple V-shaped ribs) [23], and flapped V-shaped baffles [24]. These configurations are meticulously engineered to disrupt the boundary layer, facilitate

mixing, and generate flow vortices, thereby enhancing thermal efficacy across a multitude of applications.

Wang et al. [25] studied to enhance solar cell efficiency with increasing power intensity, a microchannel heat sink with V-ribs and water-based nanofluid coolant was designed. Numerical simulations (Reynolds number 200–1000) revealed that V-ribs disrupt thermal boundaries, induce chaotic convection, and improve heat transfer. Optimal geometric and nanofluid parameters were identified, aiding MCHS design for micro solar cells. Okab et al. [26] analyzed the thermal performance of microchannels with sidewall dimples (0.5 mm and 1 mm) and a fillet profile on the bottom surface under laminar flow (Re 200–1200). Results indicated that dimples and the fillet profile significantly enhance thermal performance. Microchannels with 1 mm dimples exhibited a 20 % higher Nusselt number (*Nu*) but a 10 % pressure drop increase, while the fillet profile improved thermal performance without additional pressure drop. Combined, these features achieved a 60 % higher *Nu* compared to plain microchannels. In the detailed numerical study, Jia et al. [27] examined the unique microchannel heat sink design equipped with oval-shaped micro pin fins (MOPF), analyzing both the thermal and fluid's hydraulic properties across Reynolds numbers from 157 to 668. This research specified the three non-dimensional parameters width ratio (β), fin axial length ratio (α), and height ratio (γ) using the thermal enhancement factor (η) as the key performance indicator. The outcomes results indicated that MOPF significantly enhances both temperature uniformity and operational efficiency, with η peaking at certain values of α and β, though the exhibiting variations with changes in γ. At the optimal Reynolds number of 668, achieving $\alpha = 4$, $\beta = 0.3$, and $\gamma = 0.5$ resulted in the η of 1.56, thereby directing advancements in design approaches of microchannel heat exchangers, in this study.

Following numerous alterations in microchannel heat sinks (MCHS) designed to enhance thermal dissipation, considerable scholarly focus has transitioned towards the integration of rib insertions within MCHS. The incorporation of ribbed geometries within microchannels has been empirically demonstrated to augment the surface area available for thermal transfer and foster increased turbulence, thereby yielding superior thermal performance [28]. Consequently, researchers are investigating various rib configurations, including parameters such as height, morphology, and spacing, to further optimize the thermal transfer efficiency of MCHS. Recent empirical investigations suggest that the implementation of ribs can markedly enhance heat transfer rates by disrupting laminar flow regimes and facilitating enhanced fluid mixing within the channels. For instance, Qinghua Wang [29] conducted a detailed investigation of a sophisticated MCHS characterized by triangular truncated ribs, revealing that this arrangement significantly enhances fluid mixing and heat transfer, achieving a *Nu* performance factor of 1.081 while preserving a low pressure drop across the optimized rib designs. Saqib Ali [30] examined seven different rib placements within fan-shaped cavity microchannels, discovering that the configurations at the front and back notably improve flow mixing, resulting in a 19 % increase in the *Nu* when compared to standard designs.

Moreover, Milad Setareh [31] presented a hybrid nanofluid microchannel heat sink that features zigzag porous ribs, which displayed exceptional thermohydraulic performance compared to solid ribs; the best configuration, with a rib height of 0.1 mm, achieved a peak performance evaluation criterion of 1.86 across various Reynolds numbers. In a similar vein, Jiachang Nie [32] introduced an innovative cylindrical heat sink equipped with helical microchannels and porous ribs, which enhanced heat transfer by as much as 61.7 % while simultaneously decreasing entropy generation by 22.8 %, thus showcasing the effectiveness of porous structures in thermal management applications. In a separate investigation, Chuntong Li [33] examined a double-layered MCHS that employed both solid and porous ribs in conjunction with microencapsulated phase change materials, leading to a remarkable 124.56 % improvement in the figure of merit when contrasted with conventional solid rib configurations. Furthermore, Bin Li [34] documented a microchannel heat sink that featured a slant rib-quatrefoil rib arrangement, which significantly boosted heat transfer performance, resulting in a 66.6 % decrease in thermal resistance and a 131 % rise in *Nu* at a Reynolds number of 696. Lastly, Hussam Sadique [35] proposed an bio-inspired fractal microchannel heat sink design incorporating rib structures, which was refined using machine the learning techniques, yielding enhanced thermal performance with a optimal rib radius configuration of 26 % at an flow rate of 200 ml/min. Together, these studies highlight the essential contribution of rib configuration & advanced materials in improving the efficacy of MCHS for effective thermal management in high heat flux scenarios.

Employing of nanofluids as an the heat transfer fluids (HTFs) in the MCHS, which has been a focus of researchers with aiming to enhance system performance. These fluids, which is known for their superior thermophysical characteristics, bolster the heat transfer due to his increased thermal conductivity and heightened capacity to carry heat. Eneran et al. [36] have systematically reviewed the application of nanofluids in MCHS, discussing essential aspects such as thermal conductivity, stability, particle clustering, and the dynamics of particle-surface interactions. The adjustable thermophysical properties of nanofluids position them as suitable HTFs in MCHS. However, challenges such as clogging and particle accumulation are persistent issues, as indicated by Al-Baghdadi et al. [11], who noted that nanofluids might lead to blockages within MCHS. Therefore, water is recommended as the most suitable HTF for MCHS, due to its safe and effective operational characteristics.

In the preceding discussion predicated on prior studies, it has been discerned that passive techniques, particularly surface modifications, have been extensively utilized. Various configurations such as diverse flow passage shapes, pin fins within the flow, wavy channels, expansion-contraction passages, and dimpled ribs on passage sidewalls have been rigorously examined both experimentally and numerically. However, there remains an unexplored potential concerning extruded circular ribs on the sidewalls of the passage. It is postulated that extruded ribs, oriented at varying angles of attack and interspersed with gaps, could not only augment the heat transfer surface area but also induce turbulence, thereby enhancing the convective heat transfer coefficient, as evidenced in solar air heater applications [37,38]. With this expectation, similar ribs configurations in MCHS will boost convective heat transfer. Thus, the intent of this exploration is to dissect the potential enhancements in heat dissipation rates within MCHS brought about by the integration of V-shaped circular protrusion ribs on the passage sidewalls. The ramifications of varying the ribs' angle of attack from 35° to 90° on the thermal transfer and frictional attributes have been rigorously explored. Additionally, the thermohydraulic performance has been assessed to determine the optimal angle of attack for these circular extrusions V shape ribs.

2. Computational model of problem and process

2.1. Design and computational model

The computational domain for the microchannel heat sink (MCHS) in this study is intricately designed using the Ansys Workbench design module, encompassing both the MCHS structure and the heat transfer fluid as water. A three-dimensional, non-isothermal steady state environment simulates the complex interactions within the MCHS. The choice of silicon as the material of the microchannel leverages, which has the high thermal conductivity and mechanical stability, in general. Given that intricate structure of MCHS, which includes 50 the straight channels, the computational load and the time required for simulation are significant. To optimize the simulation process with the integrity of the results, the model focuses on a single microchannel, reflecting the practical approach to reduce the computational efforts. This channel's dimensions, which comprise 10 mm in length, 0.35 mm in width, and 0.2 mm in height are based on the prior experimental studies [39], ensuring that simulations parameters are both realistic and relevant as shown in Fig. 1 and listed in Table 1 also for reference. Additionally, the MCHS design incorporates V-shaped ribs with gap along the passage walls, strategically placed with variable angles of attack at 35°, 45°, 60°, 75°, and 90° to the enhance the heat transfer efficiency as shown in Fig. 2. The angles of attack (35°, 45°, 60°, 75°, and 90°) were meticulously selected to facilitate a systematic variation in rib orientation, thereby permitting a thorough analysis of their influences on flow behavior and thermal performance. This spectrum of angles encompasses lower, moderate, and elevated orientations, which allows for a clear juxtaposition of trends in heat transfer and hydraulic characteristics within the microchannel heat sink (MCHS). These various angle of attacks furnish the well-balanced foundation for a comprehending the extent to which rib orientation impacts on thermal and hydraulic efficiency, thereby aiding in an optimization of the design for improved cooling performance. The ribs are placed at a pitch of 0.4 mm, which considered based on the earlier research findings [6,15,40]. This ribs configurations not only facilitates a thorough understanding of the heat transfer characteristics but also the significantly contributes to the efficiency of the cooling mechanism by optimizing the fluid dynamics and the thermal interactions.

2.2. Conservation equations

In the context of the MCHS computational fluid dynamics (CFD) simulation, which the foundational set of equations governs the fluid flow as well as heat transfer mechanisms. These equations governed the conservation of mass, momentum, and energy iterative solutions method. This section aims to delineate and interpret each equation in the context of its impact on the fluid dynamics and heat transfer within MCHS.

Continuity eq.

$$\frac{\partial u}{\partial x}+\frac{\partial v}{\partial y}+\frac{\partial w}{\partial z}=0 \tag{1}$$

This equation ensures mass conservation in the flow field, which states that the sum of the rate of change of fluid velocity components in all spatial directions, i.e. in x, y, and z direction is zero, implying incompressibility of the heat transfer fluid, which is water in this case.

Momentum eq in x direction

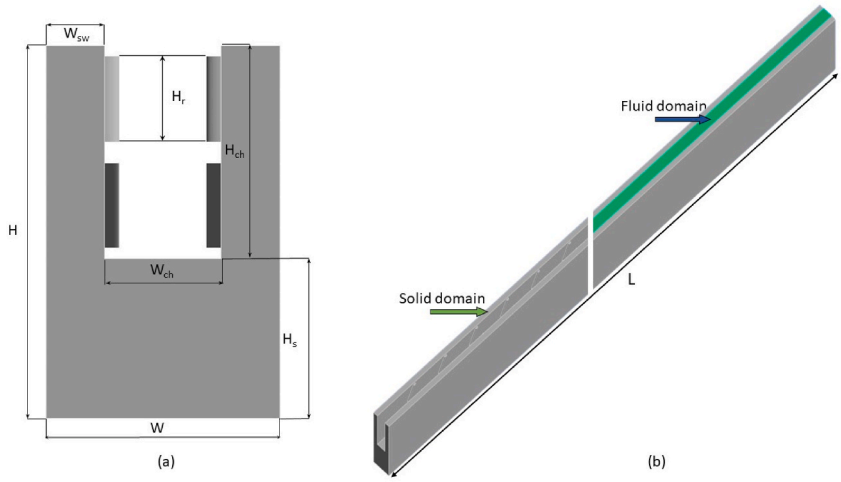

Fig. 1. (a) Cross-sectional view 3-D computational domain of single micro-channel, (b) isometric view with fluid and solid domain.

Table 1
Geometric parameter of V-shape ribs and MCHS.

No.	Parameter	Value	No.	Parameter	Value
1	H	350×10^{-6} m	6	W_{sw}	50×10^{-6} m
2	H_{ch}	200×10^{-6} m	7	L	10000×10^{-6} m
3	H_s	150×10^{-6} m	8	H_r	80×10^{-6} m
4	W	200×10^{-6} m	9	P	400×10^{-6} m
5	W_{ch}	100×10^{-6} m	10	θ	35°–90°

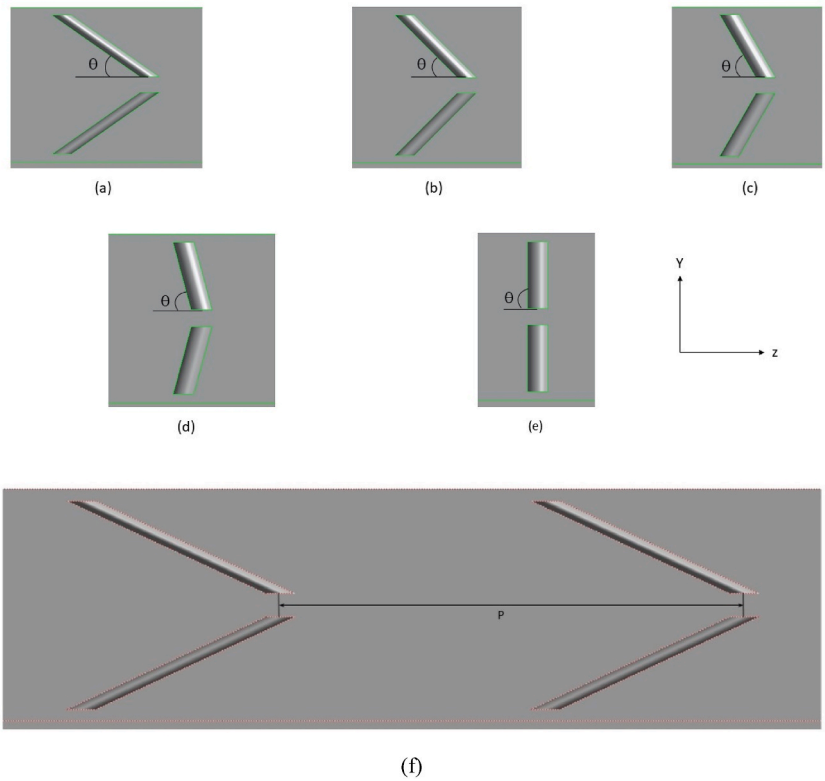

Fig. 2. View of geometry modification on passage wall surface, (a) θ = 35°, (b) θ = 45°, (c) θ = 60°, (d) θ = 75°, (e) θ = 90°, (f) pitch of V-shape rib.

$$x\frac{\partial u}{\partial x}+y\frac{\partial u}{\partial y}+z\frac{\partial u}{\partial z}=-\frac{1}{\rho_f}\frac{\partial p}{\partial x}+\frac{\mu_f}{\rho_f}\left(\frac{\partial^2 u}{\partial x^2}+\frac{\partial^2 u}{\partial y^2}+\frac{\partial^2 u}{\partial z^2}\right) \tag{2}$$

Momentum eq in y direction

$$x\frac{\partial v}{\partial x}+y\frac{\partial v}{\partial y}+z\frac{\partial v}{\partial z}=-\frac{1}{\rho_f}\frac{\partial p}{\partial y}+\frac{\mu_f}{\rho_f}\left(\frac{\partial^2 v}{\partial x^2}+\frac{\partial^2 v}{\partial y^2}+\frac{\partial^2 v}{\partial z^2}\right) \tag{3}$$

Momentum eq in z direction

$$x\frac{\partial w}{\partial x}+y\frac{\partial w}{\partial y}+z\frac{\partial w}{\partial z}=-\frac{1}{\rho_f}\frac{\partial p}{\partial z}+\frac{\mu_f}{\rho_f}\left(\frac{\partial^2 w}{\partial x^2}+\frac{\partial^2 w}{\partial y^2}+\frac{\partial^2 w}{\partial z^2}\right) \tag{4}$$

These momentum equations, based on the Navier-Stokes equations for an incompressible fluid, describe the balance between the inertial forces, the pressure gradients, and the viscous forces in the fluid.

Energy Equation (Fluid Domain):

$$u\frac{\partial T_f}{\partial x}+v\frac{\partial T_f}{\partial y}+w\frac{\partial T_f}{\partial z}=\frac{k_f}{\rho_f c_{p,f}}\left(\frac{\partial^2 T_f}{\partial x^2}+\frac{\partial^2 T_f}{\partial y^2}+\frac{\partial^2 T_f}{\partial z^2}\right) \tag{5}$$

This equation governs the temperature distribution within the fluid, which is accounting for advection and diffusion of heat. T_f represents the fluid temperature, k_f the thermal conductivity, $c_{p,f}$ the specific heat capacity, and ρf the density of a fluid.

Energy Equation (Microchannel Solid Domain):

$$k_{mc}\left(\frac{\partial^2 T_{mc}}{\partial x^2}+\frac{\partial^2 T_s}{\partial y^2}+\frac{\partial^2 s}{\partial z^2}\right)=0 \tag{6}$$

This equation describes the heat conduction within the microchannel solid domain, where T_{mc} refers temperature of the microchannel material, i.e. is silicon in this case, and k_{mc} is its thermal conductivity.

These equations are solved numerically, which predict the performance of the MCHS under various operational conditions. These governing equations are the backbone of the simulation, which providing insights into the complex phenomena of heat transfer and fluid flow within MCHS.

The following presumptions apply to the MCHS's governing equations:

i. The investigation is carried out under steady-state and laminar flow, while heat transfer fluid i.e. water considered as incompressible fluid.
ii. Thermophysical properties of the fluids considered as constant at temperature 300 K.
iii. There is no slippage between the fluid and the wall.
iv. Viscosity dissipation and radiation heat transfer effects are disregarded.
v. The fluid's gravitational forces are disregarded.

2.3. Properties of heat transfer fluid and micro-channel

The performance of the MCHS depends significantly on the thermophysical properties of both heat transfer fluid i.e. water and the microchannel material i.e. silicon. These properties influence the heat transfer efficiency and the mechanical stability of the system under different operational conditions. Water is employed as the heat transfer fluid in the MCHS due to its desirable thermophysical characteristics, which are prominent for effective thermal management. Water properties at a standard reference temperature have been summarized in Table 2. Water's high specific heat capacity and adequate thermal conductivity are the pivotal properties, which plays its role in efficiently absorbing and transporting heat away from the heat source. Its low viscosity ensures the smoother flow through the microchannels, which help to lower the pressure drops and enhancing the overall heat transfer performance. Silicon material is selected for the microchannel construction due to its mechanical along with its thermal performance characteristics. The detailed thermophysical properties of silicon have been given in Table 3. Silicon's high thermal conductivity is the key attribute, which can enhance its ability to dissipate heat in a efficient manner. Additionally, the substantial Young's moduls indicates its mechanicl strength, which is an important for maintaining structural performance under thermal stresses. The specific heat and the thermal expanson coefficient of silicon ensure, that it can be withstand and adapt temperature variation experienced during operation.

These properties of the both the heat transfer fluid and the microchannel material are critical for the design and operational efficiency of the MCHS. These interactions b/w these thermophysical properties determine the system's ability to perform under various thermal loads and environmental conditions, thereby impacting the overall effectiveness of the cooling provided by the MCHS.

2.4. Boundary conditions and numerical procedure

The numerical simulation of the MCHS employs specific boundary conditions and a detailed numerical procedure to the accurately model the fluid dynamics and the heat transfer characteristics within MCHS. The boundary conditions are set as follows: At the inlet of the MCHS, fluid is introduced with an inlet velocity that corresponds to Reynolds numbers ranging from 100 to 900, having the inlet fluid temperature maintained at 300 K. This condition allows for the simulation of laminar flow regimes, enhancing the relevance and applicability of the results across different operational scenario. At the outlet, a zero-gauge pressure condition is implemented, representing the atmospheric exit conditions and ensuring an realistic pressure gradient throughout the microchannel. A significant aspect of the thermal boundary conditions is the application of a uniform heat flux of 1×10^6 W/m^2 on the bottom wall of the MCHS, simulating the high-density heat dissipation from high-intensity electronic components. Side walls of the MCHS are treated as symmetrical, simplifying the computational domain while capturing the essence of heat transfer along the microchannels. The various boundary conditions have been visualization in Fig. 3. Regarding the numerical procedure, the simulation leverages a finite volume method facilitated by Ansys Fluent, a robust platform for tackling complex fluid flow and heat transfer problem. The velocity-pressure coupling within multi-grid solution framework is managed using the Semi-Implicit Method for Pressure Linked Equations (SIMPLE) algorithm. This approach effectively addresses coupling between the velocity as well as the pressure fields, enhancing stability and accuracy in computational the results. The iterative solution process adhere to the strigent convergence criteria, fixed at 1.0×10^{-9} for energy equation, 1.0×10^{-6} for velocity components, and 1.0×10^{-6} for momentum equation. These thresholds values ensure the simulation achieves sufficient level of precision in predicting results. This rigorous computational methodology not only the enhances

Table 2
Specialized thermophysical property assessment of water as an operative fluid.

Fluid	Thermal Conductivity k (W/m.K)	Specific Heat C_p (J/kg.K)	Dynamic Viscosity μ (Pa.s)	Density ρ_f (kg/m^3)
Water	0.600	4182.00	0.0010	998.200

Table 3
Thermophysical characteristics of MCHS.

Material	Young's Modulus Es (Pa)	Thermal Expansion β (1/K)	Thermal Conductivity ks (W/m·K)	Specific Heat Cps (J/kg·K)	Poisson's Ratio α	Density ρ_s (kg/m^3)
Silicon	170.00×10^9	2.6×10^{-6}	130.00	700.000	0.280	2329.000

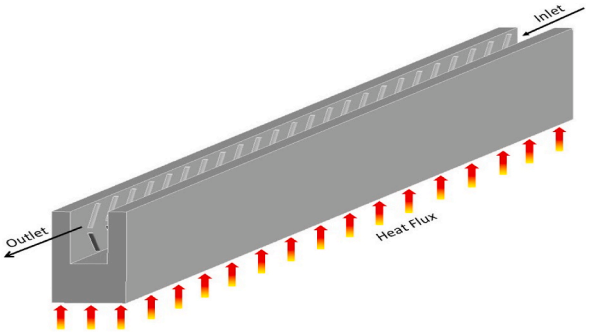

Fig. 3. Visualization of boundary conditions.

the reliability of simulation results but also shows the comprehensive understanding of thermal management capabilities of MCHS under various operting condition, thereby, supporting the design and optimization of efficient cooling solutions in electronic applications.

2.5. Mesh and its grid independent test

In the simulation of the MCHS, the precise mesh generation is an critical step, which effect the accuracy and efficiency of the computational analysis. A 3-dimensional computational domain, having a single MCHS channel along with its heat transfer fluid, was initially constructed using the design module of Ansys Workbench. These domains were discretized to generate, an unstructured mesh in tetrahedral form, with an inflation layer applied on both the solid walls and within the fluid domain. These inflation layers consisted of 5 layers, each having a growth ratio of 1.2, ensuring smooth transition and detailed resolution near the wall boundaries. Additionally, it was ensured that the y + value was maintained below 1 to accurately capture near-wall flow characteristics and provide high-fidelity results for heat and mass transfer simulations. The view of the mesh generated has been shown in Fig. 4. To substantiate the accuracy and dependability of the CFD results associated with a MCHS simulation, a grid independence check was administered. This test is crucial for confirming that the numerical results are not unduly influenced by the size or distribution of the computational grid used in this simulation. The test involved analyzing the temperature distribution within the MCHS using different mesh densities, and the outcomes are summarized in a Table 4. As the mesh is refined from 1,572,630 nodes and 8,272,376 elements to 2,455,595 nodes and 12,822,593 elements, the computed temperatures T_m (mean temperature of the microchannel convective surface area) and

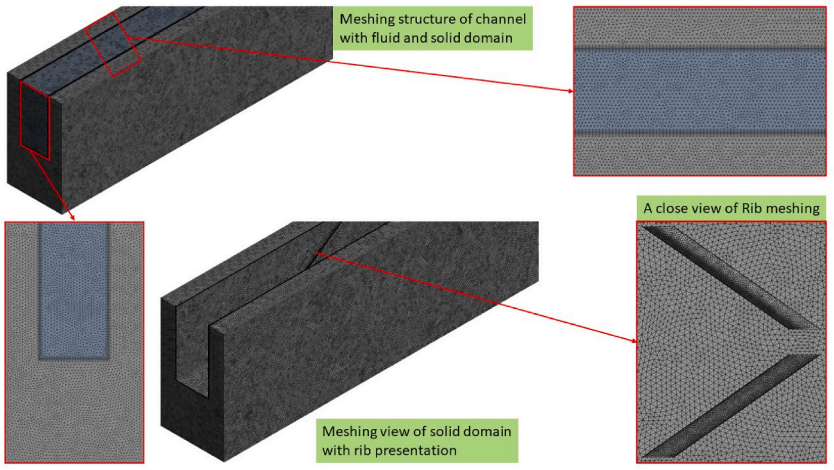

Fig. 4. Tetrahedron Meshing of fluid and MCHS domain.

Table 4
Grid independence test.

Node count	Element count	T_m	error %	T_{mb}	error %
1572630	8272376	328.59372	–	329.59287	–
2023330	10542897	329.46376	0.26	330.45186	0.26
2455595	12822593	329.5818	0.04	330.5682	0.04

T_{mb} (average passage base temp) showed a trend towards stabilization. Initially, a significant temperature shift was observed when increasing the node and element counts from the first to the second set, with an error reduction of 0.26 %. Further refinement resulted in a marginal an error of just 0.04 %, indicating that the temperatures T_m and T_{mb} are converging towards a consistent value in the simulations. This minimal change confirms that the solution is approaching grid independence, whereby further increases in the grid resolution have a negligible impact on simulations results. This test validates the mesh resolution used in the final simulations, ensuring that it can provides an optimal balance between computational resource expenditure and the accuracy required for the reliable simulated results. The established grid is thus deemed sufficient for conducting detailed analyses and for making informed decisions regarding the design and operation of the MCHS in practical the applications.

2.6. Data reduction

In the analysis of the MCHS, the reduction of experimental or simulation data into meaningful metrics is crucial for the evaluating performance characteristics such as fluid dynamics and heat transfer. The key parameters i.e., Reynolds number, hydraulic diameter, friction factor, average heat transfer coefficient, and *Nu* are derived to provide insight into the behavior of the heat sink. Here is a discussion of each term and its the significance:

Reynolds number:

$$Re = \frac{\rho_f \cdot u_m \cdot D_h}{\mu_f} \tag{7}$$

The hydraulic diameter

$$D_h = \frac{2 \cdot Wch \cdot Hch}{Wch + Hch} \tag{8}$$

The hydraulic diameter D_h is used to the characterize the dimension of non-circular conduits, such as the rectangular channels typically found in MCHS. W_{ch} and H_{ch} denote the width and height of the channel, respectively. D_h is the essential for calculating Reynolds number as well as evaluating the convective heat transfer characteristics of the fluid flowing in MCHS.

Friction factor

$$\bar{f} = \frac{\Delta p \cdot D_h}{2 \cdot \rho_f \cdot L \cdot u_m^2} \tag{9}$$

The friction factor $\bar{f}$ represents, i.e. resistance to flow due to the channel surface roughness and channel dimensions, where Δp is the pressure drop, then L the length of the channel, and ρ_f the density of the fluid. This factor is crucial for determining the pumping power required and optimizing a hydraulic performance of the MCHS.

Convective heat transfer coefficient

$$\bar{h} = \frac{q \cdot A_q}{A_c \cdot (\overline{T}_c - \overline{T}_f)} \tag{10}$$

Here, $\bar{h}$ denotes the average heat transfer coefficient, q the heat flux, A_q the area over, which the heat flux is applied, A_c is the cooling surface area, $\overline{T}_c$ is the average temperature over the conjugate area, and $\overline{T}_f$ the average temperature of the coolant. This coefficient is fundamental for assessing a thermal performance of the MCHS.

Nusselt number

$$\overline{Nu} = \frac{\bar{h} \cdot D_h}{k_f} \tag{11}$$

where,

Average temperature for the conjugated area

$$\overline{T_c} = \int \frac{T dA}{dA} \tag{12}$$

Avg temp of coolant

$$\overline{T_f} = \int \frac{T\rho_f dV}{\rho_f dV} \tag{13}$$

Thermohydraulic Performance Parameter (THPP) [41] are an critical parameter for evaluating overall performance, particularly when assessing thermal as well as hydraulic efficiency together. This parameter provide both the heat transfer capability, in term of *Nu*, and as well as the fluid flow resistance, in term of f, providing a comprehensive overview of the system's operational efficiency, which is given below.

$$Thermohydraulic\ Performance\ Parameter\ (THPP) = \frac{Nu/Nu_s}{(f/fs)^{1/3}} \tag{14}$$

2.7. Model validation

Validation of the numerical model utilized in the present simulation of a smooth microchannel, which is crucial for establishing the reliability of the numerical results. For this purposes, the present numerical results in of *Nu* and f, which have been rigorously compared with experimental data provided by Chai et al. [39]. The comparison has been illustrated in Fig. 5 for the *Nu* and f respectively, shows a strong correspondence between numerical and experimental results. This validation illustrate in the accuracy of the numerical model and substantiates its capability to replicate known behaviors in the microchannel heat transfer and fluid flow dynamics. Consequently, the validated model is deemed robust and reliable for conducting further simulations is to explore and optimize microchannel designs.

3. Results and discussion

The CFD simulation of MCHS with V-ribbed side walls at a angle of attack of 35°, 45°, 60°, 75°, and 90° have been conducted to explore the thermal as well as fluid dynamic performance across a range of operational conditions. The simulations are performed for Reynolds numbers varying from 100 to 900, which correspond to different fluid velocities, ensuring that the flow conditions set to laminar regimes. A constant and uniform heat flux of 1×10^6 W/m^2 is applied to the base of the MCHS to simulate the thermal load conditions typically applied in high-performance electronic cooling applications. To facilitate a comprehensive analysis of the results, contours of velocity, pressure, and temperature within the MCHS have been meticulously generated as well as examined. These contors provide insights into the flow dynamics and heat transfer mechanisms, highlighting the effects of rib orientation and spacing on the thermal performance and fluid flow characteristics of heat sinks. Further, the numerical data is quantitatively analyzed through the evaluation of the *Nu*, f, and pressure drop. These performance parameters plays a critical role for evaluating the efficiencies of heat transfer enhancements and the hydraulic penalties incurred due to the ribs. The numerical results thus, then serve as an robusst basis for assessing the trade-offs between improved heat transfer and increased flow resistance, guiding the optimization of MCHS designs for effective thermal management in the various engineering application.

3.1. Velocity contour

The velocity contour within the mid-plane of a microchannel heat sink (MCHS) featuring V-shaped ribs highlights the influence of rib angle of attack on fluid dynamics, particularly under Reynolds numbers (Re) of 300 and 900, as illustrated in Fig. 6. As the angle of attack of the V ribs increases from 35° to 90°, the maximum observed velocity rises significantly for both Reynolds numbers due to a more pronounced channeling effect that reduces the flow area at specific points, thereby accelerating the fluid through these

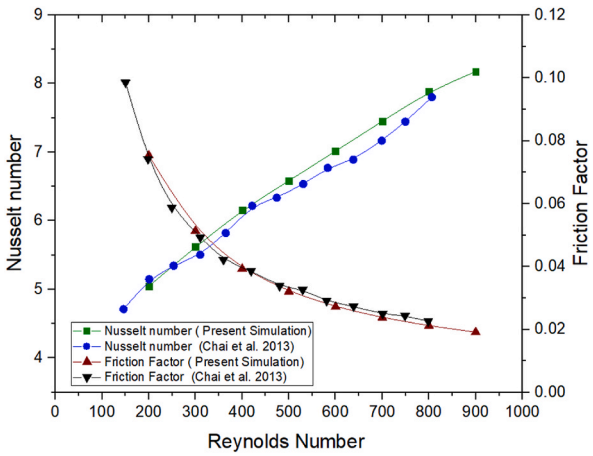

Fig. 5. Comparison of numerical results with experimental results.

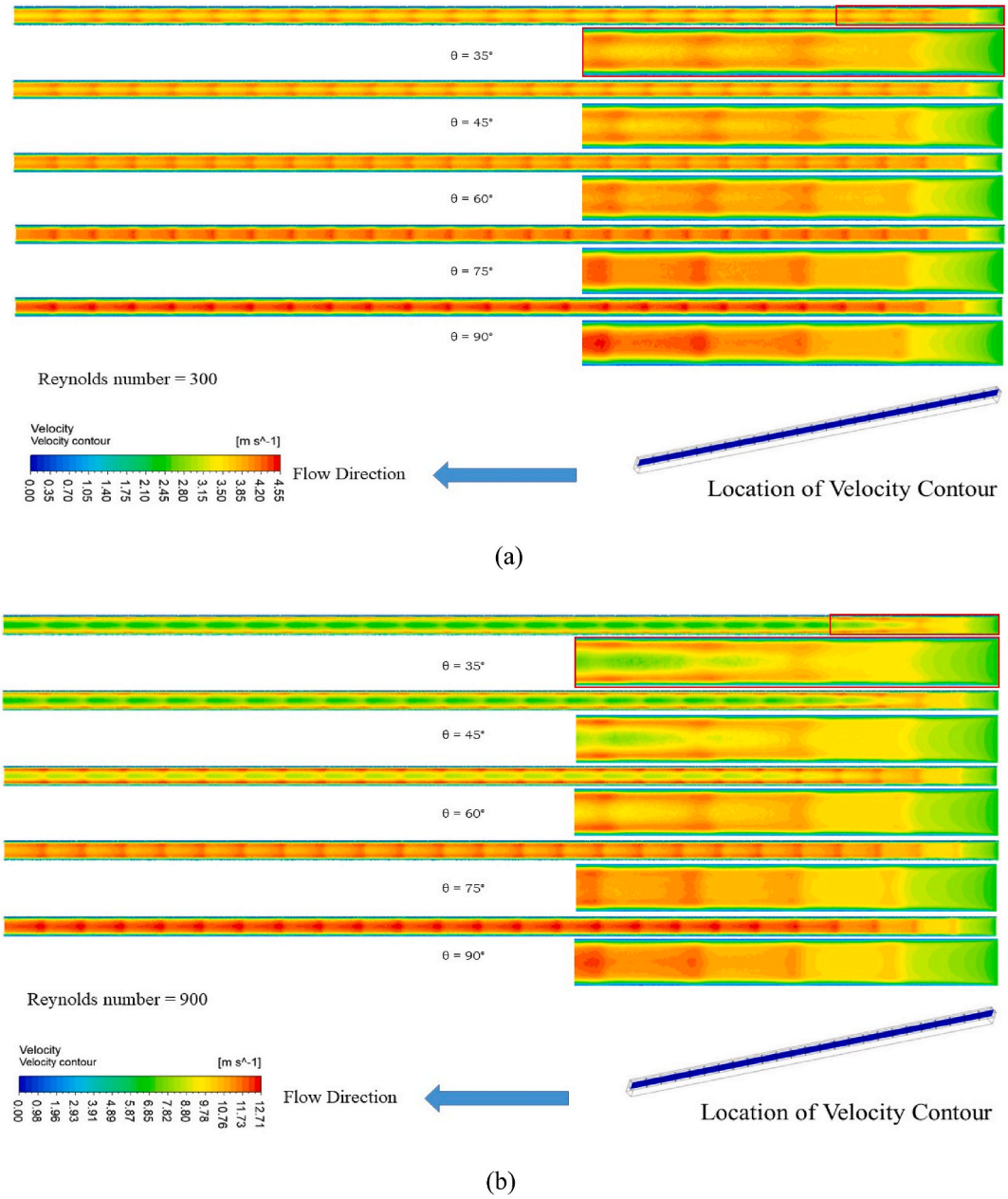

Fig. 6. Contour of velocity distribution at mid plane in micro-channel at (a) Reynold no. 300 (b) Reynold no. 900.

constricted sections. At lower angles, particularly 35°, the flow remains smoother with minimal disruption in comparison to higher angles, which introduce greater restriction, increasing local flow velocity. This effect is significant at a higher Reynolds number of 900 due to the higher fluid inertia, which amplifies the constriction effects. The resulting increase in velocity enhances convective heat transfer by thinning the thermal boundary layer, thereby improving the efficiency of the heat sink. The mid-plane velocity contour captures these dynamics well, illustrating the increase in fluid speed through tighter passages formed by steeper V ribs.

The velocity vectors within MCHS provide key insights into how the fluid flow is influenced by the structural configuration and flow conditions. Fig. 7 illustrates the velocity vector distribution near the microchannel's side walls at Reynolds numbers 300 and 900. At Re 300, the vectors are relatively uniform and parallel to the channel walls, indicating a laminar, smooth flow regime with minimal disturbances—ideal for steady-flow applications. Conversely, at Re 900, the vectors exhibit significant magnitude and direction variation, showing increased turbulence around structural features like ribs or bends, as evidenced by chaotic and scattered patterns. This turbulent flow enhances mixing and heat transfer but also contributes to increased pressure losses due to the higher energy dissipation in flows. Interestingly, the angle of attack of the V ribs significantly influences the turbulence intensity within the

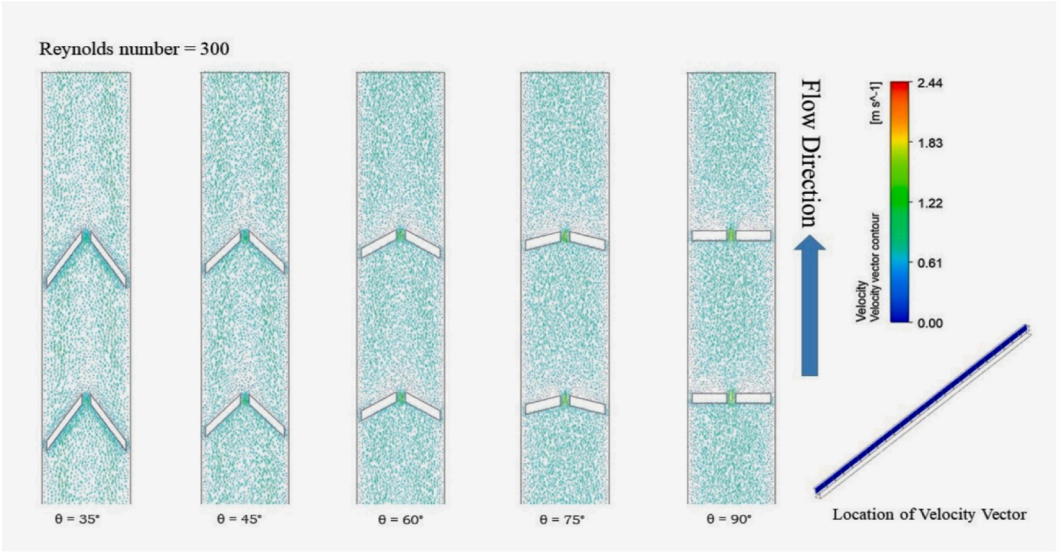

(a)

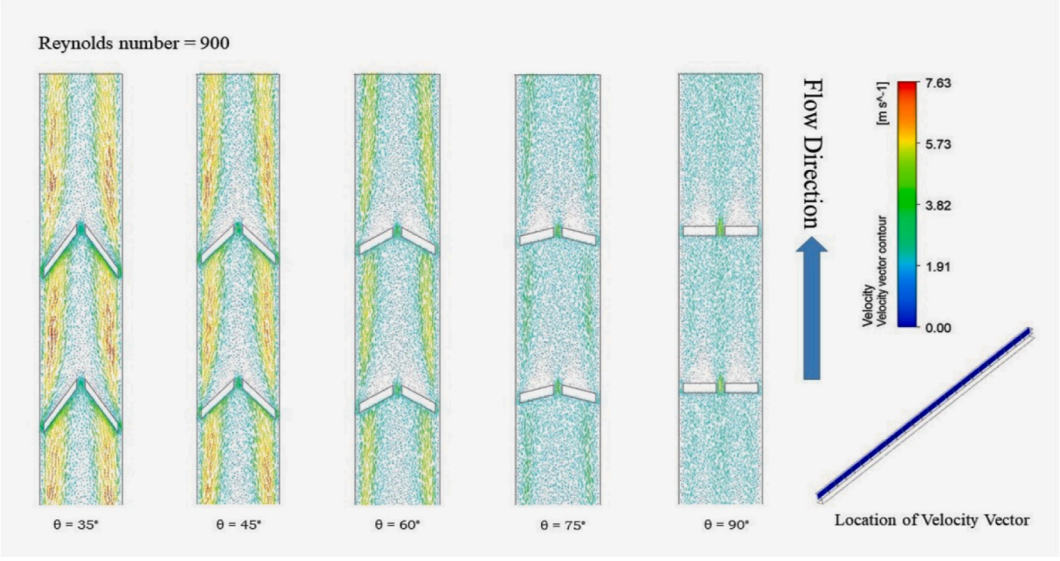

(b)

Fig. 7. Velocity vector of flow in micro-channel near to side walls at (a) Reynold no.300 (b) Reynold no. 900.

microchannel. An 35° of attack creates more turbulence compared to higher angles. This phenomenon is likely, since at a lower angle, the flow encounters the ribs more directly, causing abrupt change in direction and speed, which enhances turbulence. As the angle of attack increase, the ribs align more closely along with the flow direction, reducing the disruption and thereby diminishing the turbulence intensity. This effect is clearly demonstrated in the velocity vector distributions, which show less chaotic patterns as an angle of attack increases, suggesting a smoother flow and potentially lower the thermal performance but improved the pressure characteristics. These insights are crucial for optimizing the rib geometry to balance the heat transfer enhancement with the fluid dynamic losses, tailoring the MCHS design to specific operational needs and efficiency requirements.

3.2. Pressure contour

Pressure contour analysis within a microchannel heat sink (MCHS) equipped with V-shaped ribs reveals how variations in the angle of attack impact fluid dynamics and pressure distribution, particularly under different flow conditions (Reynolds numbers 300 and 900) as show in Fig. 8. At the lower Reynolds number (Re = 300), pressure contours display uniformity (minimal pressure drop),

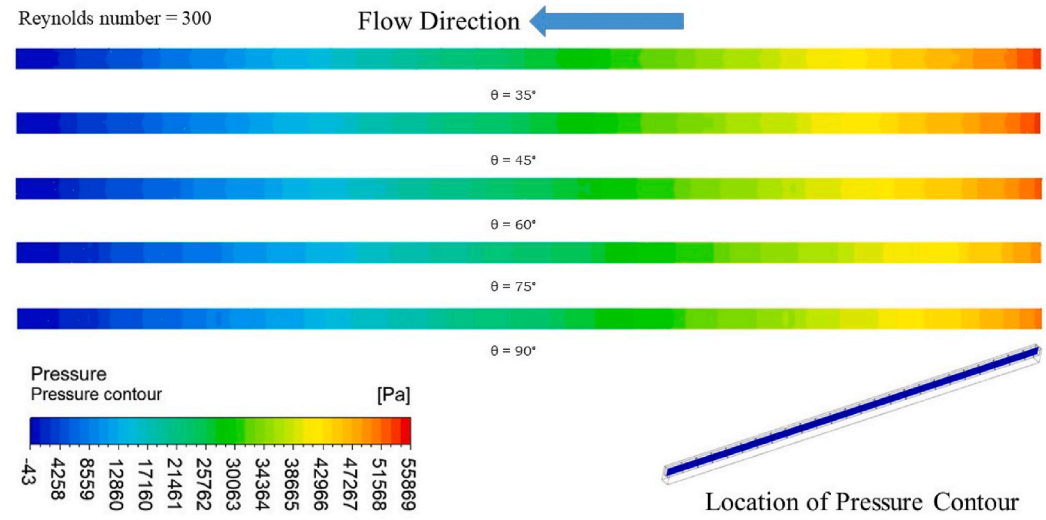

(a)

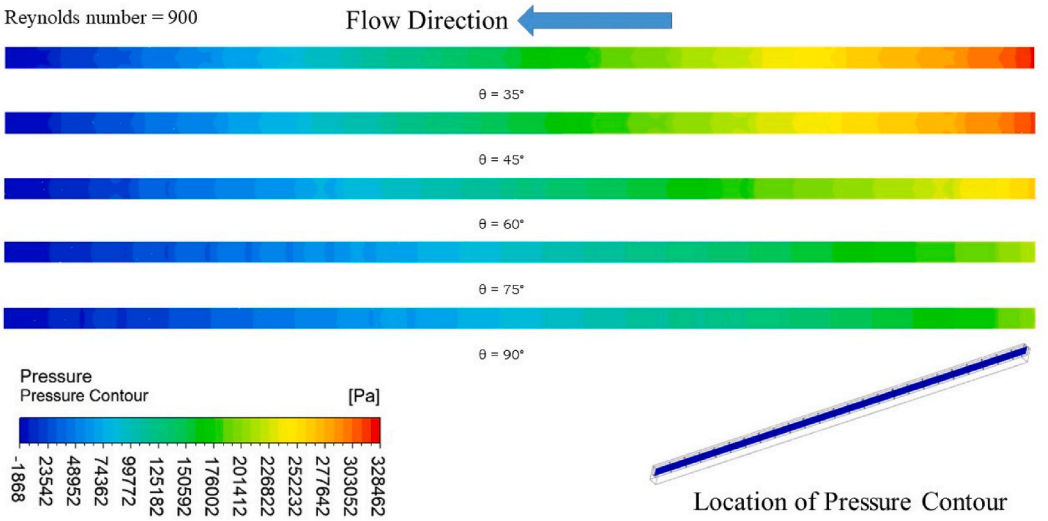

(b)

Fig. 8. Contour of pressure distribution on the mid plane of flow of micro-channel at (a) Reynold no. 300 (b) Reynold no. 900.

indicative of laminar flow with minimal disturbances and pressure losses. This scenario suits applications needing efficient, low-energy fluid flow. Conversely, at the higher Reynolds number (Re = 900), pressure contours exhibit greater complexity due to increased dynamic pressure changes from flow disruptions caused by the ribs. These disruptions lead to higher local pressure gradients and overall pressure losses, characteristic of systems requiring rapid heat removal but facing higher hydraulic resistance. A notable finding is that a 35° angle of attack generates significant pressure drops across both flow regimes, attributed to the more perpendicular interaction between the flow and ribs. This orientation enhances turbulence, leading to greater momentum exchange and energy dissipation. However, as the angle increases, the ribs become perpendicular with the flow, reducing turbulence and associated pressure drops. This demonstrates a trade-off in MCHS design between enhancing heat transfer through increased turbulence and managing pressure losses for operational efficiency. Such insights guide the optimization of rib geometry to balance thermal performance with fluid dynamic considerations.(a)

3.3. Temperature distribution

The temperature distribution within a microchannel heat sink (MCHS) is critically influenced by the flow conditions and the geometrical configuration of the V-shaped ribs, as demonstrated by the contours of temperature gradients at the base of the micro-channel as shown in Fig. 9 for Reynolds numbers 300 and 900. The temperature contour is vital for evaluating the MCHS's heat transfer efficiency and thermal management capabilities under different operating conditions. At a Reynolds number of 300, the contours demonstrate a gradual and uniform gradient, signifying efficient heat conduction with minimal convective heat transfer, characteristic of laminar flow, leading to a steady temperature profile suited for stable thermal conditions. In contrast, at Re 900, steeper temperature gradients emerge due to heightened heat transfer driven by turbulence, disrupting the thermal boundary layer more effectively. Additionally, an increase in the V-shaped rib angle of attack from 35° to 90° results in a rise in temperature along the microchannel base. This phenomenon can be attributed to several factors. Firstly, at higher angles of attack, the ribs become more perpendicular to

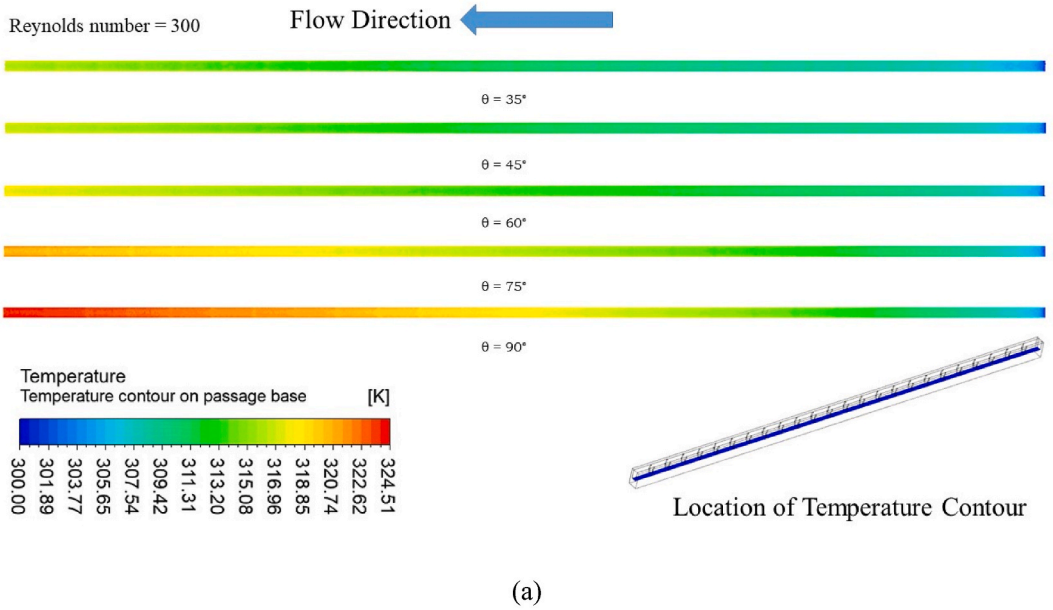

Fig. 9. Contour of temperature gradient at base of micro-channel at (a) Reynold no. 300 (b) Reynold no. 900.

the flow direction, which can reduce the turbulence intensity that facilitates heat dispersion. This alignment may lower the fluid's mixing efficiency, resulting in less effective heat transfer from the microchannel walls to the fluid. Additionally, the increased angle of attack can influence the flow velocity distribution and local fluid dynamics, further impacting the convective heat transfer rates.

The temperature distribution within a microchannel heat sink (MCHS), particularly when influenced by the orientation of V-shaped ribs and varying flow conditions, is depicted in Fig. 10 through the contours of temperature gradients at the mid-plane of the microchannel and fluid domain for the Reynolds numbers 300 and 900. These contours provide critical insights into how changes in flow dynamics impact thermal management effectiveness. At the lower Reynolds number of 300, the temperature contours are relatively smooth and uniform, indicative of a laminar flow regime where heat conduction dominates over convective heat transfers. This uniformity in temperature distribution is then beneficial for applications requiring stable and consistent cooling performance, as it

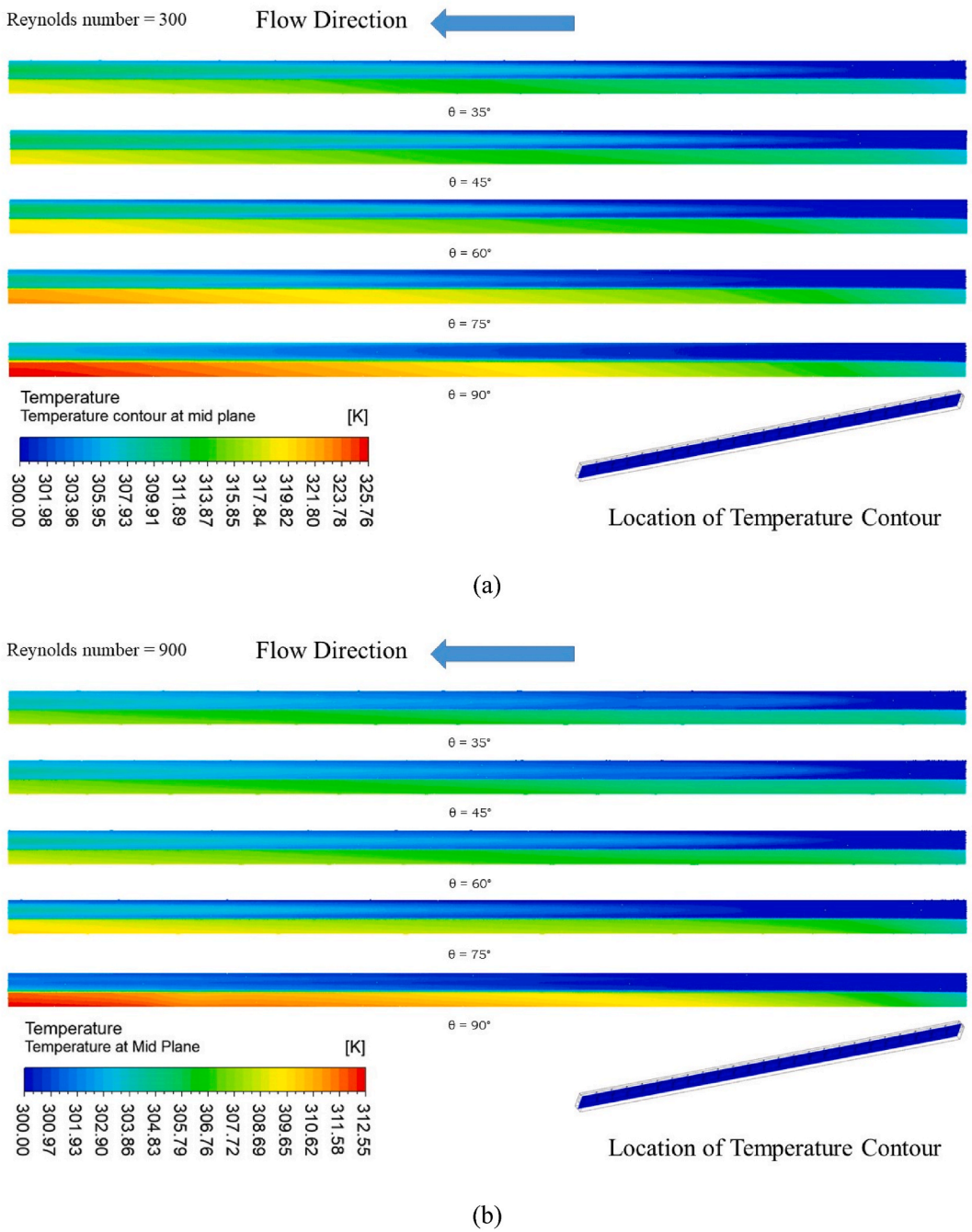

Fig. 10. Contour of temperature gradient at mid plane of micro-channel and fluid domain at (a) Reynold no. 300 (b) Reynold no. 900.

suggests minimal thermal stratification across the microchannel. Conversely, at a Reynolds number of 900, the temperature contours show the more complex and varied pattern, reflecting an increased influence of convective heat transfer due to turbulent flow. At higher flow rates i.e Re = 900, the introduction of turbulence disrupts the thermal boundary layer, promoting more effective heat transfer from the microchannel walls to the fluid. However, this also creates more pronounced temperature gradients, which, if not properly managed, could result in hotspots. Additionally, as the angle of attack increases from 35° to 90°, aligning the ribs perpendicular to the flow, these effects become more significant. The perpendicular rib orientation introduces greater flow obstruction and turbulence, enhancing heat transfer but also increasing the likelihood of uneven temperature distributions and localized overheating.

The temperature distribution on the side passage walls within a microchannel heat sink (MCHS) under various angles of attack (θ) and Reynolds numbers (Re = 300 and 900) is critically analyzed using the data presented in Fig. 11. This Figs. illustrate how different rib orientations affect thermal management along the sidewalls surface contours of the MCHS. At the lower Reynolds number (300), the temperature distribution is more uniform across all angles of attack, suggesting that heat conduction is more dominant under

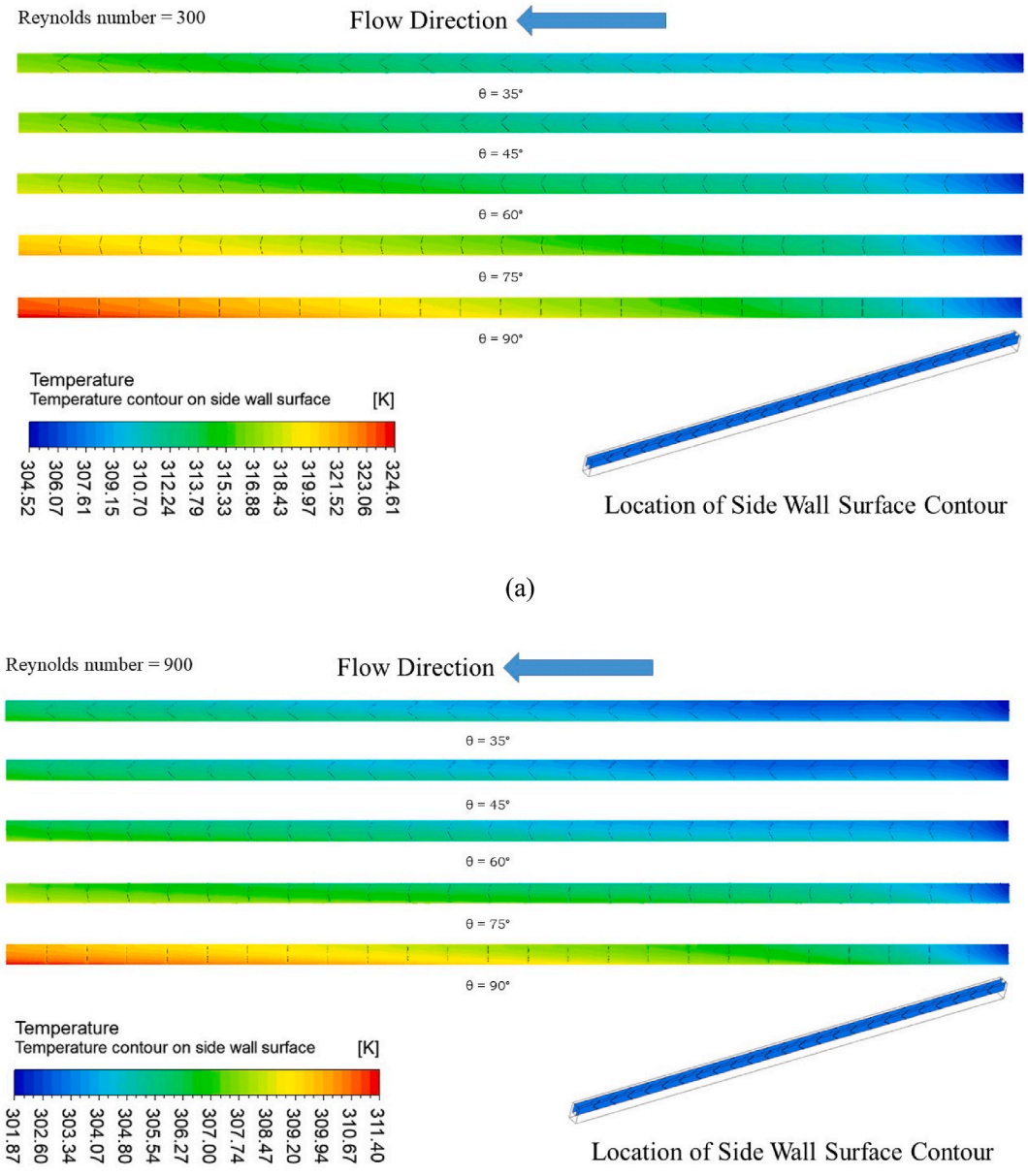

Fig. 11. Contour of temperature gradient of side walls of passage in micro-channel at (a) Reynold no. 300 (b) Reynold no. 900.

laminar flow conditions. This uniformity is beneficial for applications that require stable thermal conditions without significant variations in temperature. The minimal impact of angle variations at this lower flow rate indicates the controlled thermal environment, which is ideal for precise thermal management tasks. On the other hand, at the higher Reynolds number (900), the temperature contours become increasingly complex as the angle of attack increases. Starting from a 35° angle up to a 90° angle, there is a noticeable shift in temperature gradients. Particularly at 90°, where the ribs are perpendicular to the flow direction, there is significant turbulence, which disrupts the thermal boundary layer more aggressively. This leads to enhanced convective heat transfer, making the cooling process more efficient but also more variable, which could lead to potential hotspots if not properly managed.

3.4. Performance matrix of micro-channel heat sink

Analyzing the *Nu* across different angles of attack in a microchannel heat sink (MCHS) provides a clear perspective on how rib orientation impacts heat transfer efficiency, particularly when coupled with varying Reynolds numbers. Fig. 12 displays *Nu* values for angles from 35° to 90°, alongside a smooth channel baseline, across Reynolds numbers from 100 to 900. Ribs significantly increase the *Nu* compared to the smooth configuration across all studied conditions, highlighting their effectiveness in enhancing convective heat transfer due to increased surface area and induced turbulence. For instance, at a Reynolds number of 100, the *Nu* for a ribbed channel at 35° is 6.85, compared to 4.56 for the smooth channel, yielding an enhancement ratio of approximately 1.5. This ratio signifies an 50 % increase in the heat transfer coefficient due to the ribbed configurations. As the Reynolds number increases, the enhancement ratio also tends to increase, reflecting the ribs' role in effectively disrupting the thermal boundary layers. The highest *Nu* are recorded at the lowest angle of attack (35°) across all Reynolds numbers, gradually decreasing as an angle of attack increases to 90°. It can be seen that lower angles foster more effective turbulence for thermal mixing, increasing heat transfer more efficiently than at higher angles. The trend in temperature distribution on the base plate correlates with these findings. Lower angles of attack, which produce higher *Nu*, are associated with more effective turbulence and better thermal mixing, leading to a more uniform and lower base plate temperature. At 90°, the perpendicular alignment of the ribs to the flow, despite causing significant turbulence, may not allow for as effective thermal mixing, as evidenced by the smaller enhancement in the *Nu* compared to lower angles. These insights emphasize that while ribs significantly improve heat transfer compared to smooth channels, the angle of attack must be optimized to balance turbulence with efficient heat exchange. Lower angles (around 35°) appear optimal, enhancing heat transfer significantly without excessive resistance or overheating, crucial for maximizing the thermal performance of MCHS across various applications.

Fig. 13 shows the variation of temperature at the base of the microchannel heat sink (MCHS) passage for different angles of attack provides a clear indication of how rib orientation impacts thermal performance across various Reynolds numbers, ranging from 100 to 900. These temperatures at angles from 35° to 90° are compared to a smooth channel to understand the effect of rib-induced turbulence and heat transfer enhancements. As shown, the temperature at the base of the passage consistently decreases as the angle of attack decreases from 90° to 35° across all Reynolds numbers. This trend is a direct consequence of the increased turbulence and enhanced heat transfer capabilities at lower angles of attack, as previously observed in the temperature contours. At a 90° angle, where ribs are perpendicular to the flow, they create significant turbulence, which, while enhancing heat transfer, also localizes heat due to the direct obstruction and resistance to flow, leading to higher base temperatures. Conversely, at lower angles like 35°, the ribs align more with the flow direction, reducing direct obstruction and allowing a smoother flow with less localized heating, thereby lowering the temperature. This phenomenon aligns with the observed temperature contours on the base of the passage, where less steep rib angles facilitated better thermal management by reducing the severity of hotspots and distributing the heat more evenly across the passage.

The variation of f at different angles of attack in a microchannel heat sink (MCHS) illustrates the relationship between ribs configurations and flow resistance, especially under varying Reynolds numbers. As shown in Fig. 14, f for ribbed channels at angles from

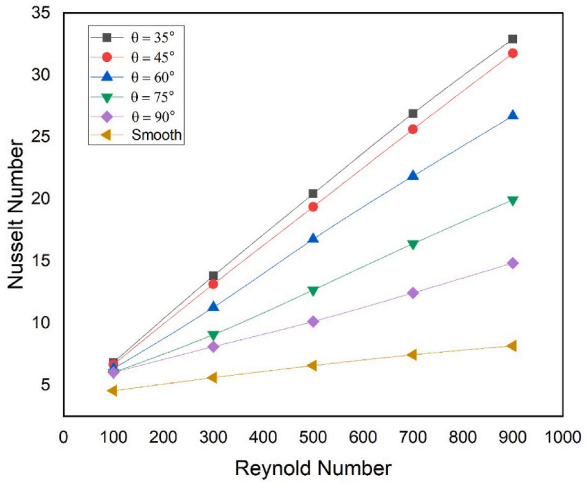

Fig. 12. Nusselt number of micro-channel heat sink varies with Reynold numbers for different angle of attack.

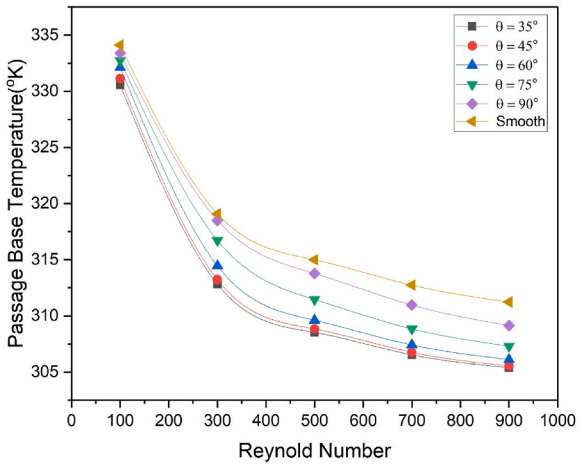

Fig. 13. Temperature variation of the micro-channel heat sink at base of passage with varying angle of attack.

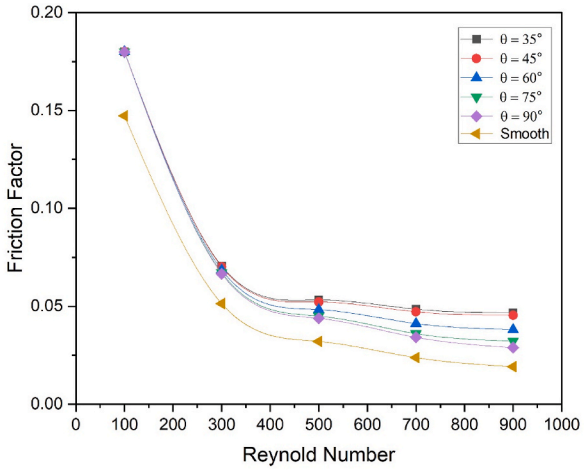

Fig. 14. Friction factor in Micro-channel heat sink varies with Reynolds number for different angle of attack.

35° to 90° are compared with those for a smooth channel configuration across Reynolds numbers from 100 to 900. At each Reynolds number, the f for ribbed channels is significantly higher than that for the smooth channel. This increase in f can be attributed to the ribs' impact on the flow path, creating more surface area and obstacles that the fluid must navigate, thereby increasing the flow resistance. The data shows that as the angle of attack increases from 35° to 90°, the f generally decreases, suggesting that the flow encounters less resistance as the ribs oriented perpendicular the flow direction, minimizing disruptions. This trend is consistent with the previously discussed pressure contours as presented in Fig. 8, where higher angles of attack (approaching 90°) showed a decrease in pressure drop across the channel. This relationship indicates that while perpendicular ribs (at 90°) generate significant turbulence, they may not obstruct the flow as much as ribs at lower angles, such as 35°, where the flow faces more direct resistance. This increased obstruction at lower angles results in higher friction factors (f) and consequently greater pressure drops, as evident in the contours. The observed reduction in f with increasing angles of attack suggests that although turbulence, which is beneficial for heat transfer, is enhanced, the direct resistance to flow decreases as the ribs align closer to the flow direction. Therefore, optimizing the rib angle requires not only maximizing heat transfer, as reflected by variations in the Nusselt number (*Nu*), but also carefully balancing flow resistance to ensure an efficient and effective cooling system. This balance is crucial for designing MCHS that achieve desired thermal management outcomes without excessively burdening the system's hydraulic performance.

The analysis of pumping power requirements across different angles of attack in a microchannel heat sink (MCHS) equipped with V-shaped ribs offers crucial insights into the operational efficiency and hydraulic demands of the system under varied flow conditions as shown in Fig. 15. The provided data spans Reynolds numbers from 100 to 900, comparing the energy needed to maintain flow in channels with V-shaped ribs at angles from 35° to 90° against a smooth channel configuration. Across all tested conditions, channels with V-shaped ribs consistently require more pumping power than the smooth configuration. This increased demand is primarily due to the added flow resistance introduced by the V-shaped ribs, which necessitates greater energy to sustain the desired flow rate. Notably, as the angle of attack increases from 35° to 90°, there's a discernible reduction in pumping power requirements. This trend

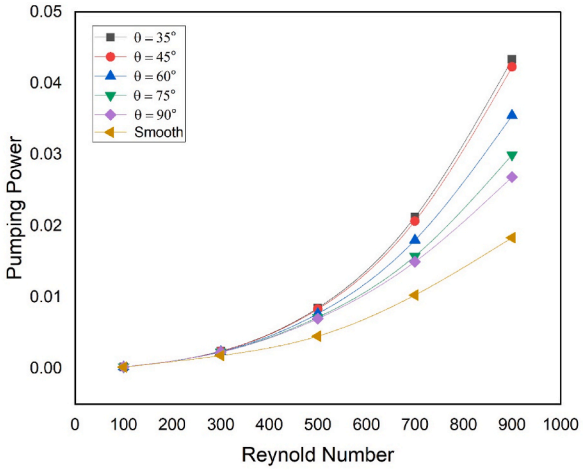

Fig. 15. Pumping power requirements in micro-channel heat sink with Reynolds number for different angle of attack.

suggests that V-shaped ribs at higher angles provide less resistance to flow by aligning more perpendicular to the flow direction, then minimizing direct obstruction and the associated turbulence. This observation aligns well with the previously discussed pressure contours, where higher angles like 90° resulted in lower pressure drops across the channel compared to more acute angles. At an 90° angle, the V-shaped ribs, being perpendicular to the flow, disrupt the flow less than at lower angles, where they significantly impede the flow path and enhance turbulence. Consequently, while perpendicular V-shaped ribs may improve turbulence beneficial for heat transfer, they may paradoxically not significantly increase pumping power requirements due to their orientation, which reduces prolonged contact with the flowing fluid. Therefore, selecting an angle that balances the benefits of increased heat transfer with the manageable pumping power requirements is crucial for optimizing the performance of MCHS. This balance ensures that the system not only performs effectively in terms of cooling but also operates efficiently, maintaining operational costs at reasonable levels.

The thermohydraulic performance parameter (THPP) evaluates the effectiveness and efficiency of MCHS with V-shaped ribs under varying angles of attack for Reynolds numbers ranging from 100 to 900. This parameter integrates thermal performance, indicated by the *Nu*, and hydraulic performance, reflected by the f, providing a holistic view of the system's overall performance. Data shows THPP values for angles of attack from 35° to 90° as a function of Reynolds number, as shown in Fig. 16. There is a discernible trend where THPP decreases as the angle of attack increases across all Reynolds numbers. This pattern underscores the delicate balance required between enhancing heat transfer and managing flow resistance within the MCHS. At a 35° angle of attack, THPP is the highest, suggesting an optimal balance in achieving efficient heat transfer with manageable pumping power requirements. Conversely, as the angle of attack reaches 90°, the THPP value declines, indicating a reduction in performance efficiency, likely due to increased flow resistance overshadowing the benefits of heat transfer enhancement. This trend corresponds with previously discussed changes in the values of the *Nu* and f. At lower angles of attack, the higher *Nu* suggest better heat transfer capabilities, positively influencing the THPP values. However, with an increasing angle of attack, the advantages of enhanced heat transfer are mitigated by the increased energy

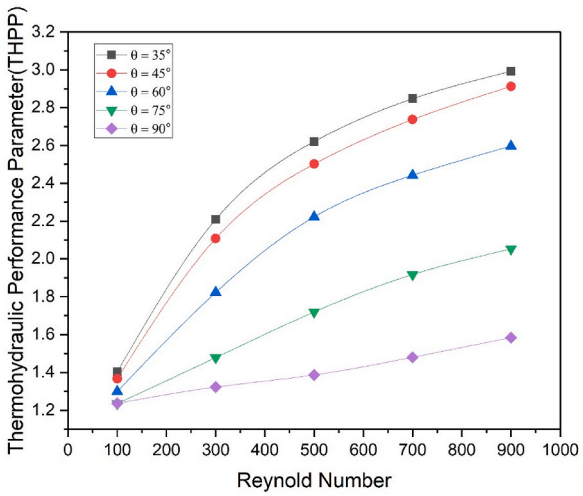

Fig. 16. Thermo–hydraulic performance parameter of micro-channel heat sink variation with Reynolds number for different angle of attack.

demand needed to overcome hydraulic resistance, which has been seen in rising f values. For example, at a Reynolds number of 300, THPP decreases from 2.21 at a 35° angle of attack to 1.32 at a 90° angle of attack, reflecting a decrease in the *Nu* benefits relative to the increase in the f.

4. Conclusions

This research thoroughly examined the effects of V-shaped rib angles of attack on the thermal and hydraulic efficiency of microchannel heat sinks (MCHS) within a Reynolds number range of 100–900. The findings indicate that a smaller angle of attack, especially at 35°, markedly improves thermal performance, with the peak *Nu* reaching 13.81 and a base temperature of 312.82 K at a Reynolds number of 300, in contrast to 8.11 and 318.51 K at 90°. This enhancement underscores the contribution of increased turbulence at reduced angles in facilitating heat dissipation. Nevertheless, lower angles also resulted in elevated f, necessitating higher energy input for fluid flow. At a Reynolds number of 900, the f was 0.0465 at 35°, compared to 0.0288 at 90°, illustrating the compromise between heat transfer and hydraulic efficiency.

In conclusion, optimal thermal efficiency in MCHS is attained at reduced angles, where the interplay between enhanced heat transfer and fluid resistance is advantageous. These results offer essential insights into rib angle selection for cutting-edge cooling applications that demand meticulous thermal management.

CRediT authorship contribution statement

Naushad Ali: Writing – review & editing, Writing – original draft, Visualization, Methodology, Formal analysis, Conceptualization. **Injamamul Haque:** Writing – review & editing, Methodology, Investigation. **Tabish Alam:** Writing – review & editing, Writing – original draft, Supervision, Methodology, Formal analysis. **Tauseef Uddin Siddiqui:** Writing – review & editing, Formal analysis. **Mushtaq Ahmad Ansari:** Writing – review & editing, Supervision. **Jagmohan Yadav:** Writing – review & editing, Conceptualization. **Shivam Srivastava:** Writing – review & editing, Formal analysis. **Erdem Cuce:** Writing – review & editing, Supervision, Methodology. **Intesaaf Ashraf:** Writing – review & editing. **Dan Dobrotă:** Writing – review & editing, Supervision.

Declaration of competing interest

The authors declare that they have no known competing financial interests or personal relationships that could have appeared to influence the work reported in this paper.

Acknowledgements

The authors acknowledge and extend their appreciation to the Researchers Supporting Project Number (RSPD2024R996), King Saud University, Riyadh, Saudi Arabia, for funding this study.

Data availability

Data will be made available on request.

References

[1] S. Ndao, Y. Peles, M.K. Jensen, Multi-objective thermal design optimization and comparative analysis of electronics cooling technologies, Int. J. Heat Mass Tran. 52 (2009) 4317–4326, https://doi.org/10.1016/j.ijheatmasstransfer.2009.03.069.
[2] I.K. Karathanassis, E. Papanicolaou, V. Belessiotis, G.C. Bergeles, Multi-objective design optimization of a micro heat sink for Concentrating Photovoltaic/Thermal (CPVT) systems using a genetic algorithm, Appl. Therm. Eng. 59 (2013) 733–744, https://doi.org/10.1016/j.applthermaleng.2012.06.034.
[3] W. Dong, X. Zhang, B. Liu, B. Wang, Y. Fang, Research progress on passive enhanced heat transfer technology in microchannel heat sink, Int. J. Heat Mass Tran. 220 (2024) 125001, https://doi.org/10.1016/j.ijheatmasstransfer.2023.125001.
[4] L. Du, W. Hu, An overview of heat transfer enhancement methods in microchannel heat sinks, Chem. Eng. Sci. 280 (2023) 119081, https://doi.org/10.1016/j.ces.2023.119081.
[5] G. Song, H. Chen, Y. Zhang, J. Wei, X. Ma, Reviews: applications of optimization algorithm for microchannel and microchannel heat sink on heat transfer, Int. J. Heat Fluid Flow 108 (2024) 109451, https://doi.org/10.1016/j.ijheatfluidflow.2024.109451.
[6] N. Kumari, T. Alam, M.A. Ali, A.S. Yadav, N.K. Gupta, M.I.H. Siddiqui, et al., A numerical investigation on hydrothermal performance of micro channel heat sink with periodic spatial modification on sidewalls, Micromachines (Basel) 13 (2022) 1986.
[7] Y. Jia, J. Huang, J. Wang, H. Li, Heat transfer and fluid flow characteristics of microchannel with oval-shaped micro pin fins, Entropy 23 (2021), https://doi.org/10.3390/e23111482.
[8] I. Kotcioglu, S. Caliskan, A. Cansiz, S. Baskaya, Second law analysis and heat transfer in a cross-flow heat exchanger with a new winglet-type vortex generator, Energy 35 (2010) 3686–3695, https://doi.org/10.1016/j.energy.2010.05.014.
[9] D.J.H. Graduate, Optimal thermal design of forced conwection, Heat Sinks-Anal. 113 (1991) 313–321.
[10] K. Derakhshanpour, R. Kamali, M. Eslami, Effect of rib shape and fillet radius on thermal-hydrodynamic performance of microchannel heat sinks: a CFD study, Int. Commun. Heat Mass Tran. 119 (2020), https://doi.org/10.1016/j.icheatmasstransfer.2020.104928.
[11] M.A.R. Sadiq Al-Baghdadi, Z.M.H. Noor, A. Zeiny, A. Burns, D. Wen, CFD analysis of a nanofluid-based microchannel heat sink, Therm. Sci. Eng. Prog. 20 (2020) 100685, https://doi.org/10.1016/j.tsep.2020.100685.
[12] V. Yadav, K. Baghel, R. Kumar, S.T. Kadam, Numerical investigation of heat transfer in extended surface microchannels, Int. J. Heat Mass Tran. 93 (2016) 612–622, https://doi.org/10.1016/j.ijheatmasstransfer.2015.10.023.

[13] R. Sabbah, M.M. Farid, S. Al-Hallaj, Micro-channel heat sink with slurry of water with micro-encapsulated phase change material: 3D-numerical study, Appl. Therm. Eng. 29 (2009) 445–454, https://doi.org/10.1016/j.applthermaleng.2008.03.027.
[14] N. Ali, S. Srivastava, I. Haque, J. Yadav, T. Alam, T.U. Siddiqui, et al., Heat dissipation and fluid flow in micro-channel heat sink equipped with semi-elliptical pin-fin structures: a numerical study, Int. Commun. Heat Mass Tran. 155 (2024) 107492, https://doi.org/10.1016/j.icheatmasstransfer.2024.107492.
[15] A.P. Dash, T. Alam, M.I.H. Siddiqui, P. Blecich, M. Kumar, N.K. Gupta, et al., Impact on heat transfer rate due to an extended surface on the passage of microchannel using cylindrical ribs with varying sector angle, Energies (Basel) 15 (2022) 8191.
[16] S. Saha, T. Alam, M.I.H. Siddiqui, M. Kumar, M.A. Ali, N.K. Gupta, et al., Analysis of microchannel heat sink of silicon material with right triangular groove on sidewall of passage, Materials 15 (2022), https://doi.org/10.3390/ma15197020.
[17] R. Wang, W. Wang, J. Wang, Z. Zhu, Analysis and optimization of trapezoidal grooved microchannel heat sink using nanofluids in a micro solar cell, Entropy 20 (2018), https://doi.org/10.3390/e20010009.
[18] T.K. Nandi, H. Chattopadhyay, Numerical investigations of simultaneously developing flow in wavy microchannels under pulsating inlet flow condition, Int. Commun. Heat Mass Tran. 47 (2013) 27–31, https://doi.org/10.1016/j.icheatmasstransfer.2013.06.008.
[19] H. Babar, H. Wu, H.M. Ali, T.R. Shah, W. Zhang, Staggered oriented airfoil shaped pin-fin heat sink: investigating the efficacy of novel water based ferric oxide-silica hybrid nanofluid, Int. J. Heat Mass Tran. 194 (2022), https://doi.org/10.1016/j.ijheatmasstransfer.2022.123085.
[20] V.R. Sharma, S.S. S, N. Madhwesh, M.S. Manjunath, Enhanced thermal performance of tubular heat exchanger using triangular wing vortex generator, Cogent Eng 9 (2022), https://doi.org/10.1080/23311916.2022.2050021.
[21] N. Jayranaiwachira, P. Promvonge, C. Thianpong, S. Skullong, Thermal-hydraulic performance of solar receiver duct with inclined punched-ribs and grooves, Case Stud. Therm. Eng. 39 (2022), https://doi.org/10.1016/j.csite.2022.102437.
[22] D. Jin, S. Quan, J. Zuo, S. Xu, Numerical investigation of heat transfer enhancement in a solar air heater roughened by multiple V-shaped ribs, Renew. Energy 134 (2019) 78–88, https://doi.org/10.1016/j.renene.2018.11.016.
[23] D. Jin, M. Zhang, P. Wang, S. Xu, Numerical investigation of heat transfer and fluid flow in a solar air heater duct with multi V-shaped ribs on the absorber plate, Energy 89 (2015) 178–190, https://doi.org/10.1016/j.energy.2015.07.069.
[24] P. Promvonge, S. Skullong, Thermal-hydraulic performance enhancement of solar receiver channel by flapped V-baffles, Chem. Eng. Res. Des. 182 (2022) 87–97, https://doi.org/10.1016/j.cherd.2022.03.051.
[25] R. Wang, J. Wang, W. Yuan, Analysis and optimization of a microchannel heat sink with V-ribs using nanofluids for micro solar cells, Micromachines (Basel) 10 (2019), https://doi.org/10.3390/mi10090620.
[26] A.K. Okab, H.M. Hasan, M. Hamzah, K. Egab, A. Al-Manea, T. Yusaf, Analysis of heat transfer and fluid flow in a microchannel heat sink with sidewall dimples and fillet profile, Int. J. Thermofluids 15 (2022), https://doi.org/10.1016/j.ijft.2022.100192.
[27] Y. Jia, J. Huang, J. Wang, H. Li, Heat transfer and fluid flow characteristics of microchannel with oval-shaped micro pin fins, Entropy 23 (2021), https://doi.org/10.3390/e23111482.
[28] A.P. Dash, T. Alam, M.I.H. Siddiqui, P. Blecich, M. Kumar, N.K. Gupta, et al., Impact on heat transfer rate due to an extended surface on the passage of microchannel using cylindrical ribs with varying sector angle, Energies (Basel) 15 (2022), https://doi.org/10.3390/en15218191.
[29] Q. Wang, J. Tao, Z. Cui, T. Zhang, G. Chen, Numerical simulation of fluid and heat transfer characteristics of microchannel heat sink with fan-shaped grooves and triangular truncated ribs, Int. Commun. Heat Mass Tran. 155 (2024), https://doi.org/10.1016/j.icheatmasstransfer.2024.107580.
[30] S. Ali, S. Alam, M.N. Khan, Effect of cylindrical ribs arrangement in the cavity region of the microchannel heatsink with a fan-shaped cavity, Proc. IME E J. Process Mech. Eng. (2024), https://doi.org/10.1177/09544089241231481.
[31] M. Setareh, I. Sheydayi, H. Basirat Tabrizi, M.R. Assari, A numerical study on the novel composition of porous and solid ribs to augment the thermal performance of a hybrid nanofluid-based microchannel heat sink with external fins, Iranian J. Sci. Technol.- Trans. Mech. Eng. (2024), https://doi.org/10.1007/s40997-024-00810-w.
[32] J. Nie, S. Liang, J. Liu, Z. Wang, Z. Feng, F. Guo, et al., Effects of porous material ribs on the hydrothermal performance and entropy generation in cylindrical helical microchannels heat sinks, Int. Commun. Heat Mass Tran. 152 (2024), https://doi.org/10.1016/j.icheatmasstransfer.2024.107309.
[33] C. Li, W. Chen, Thermo-hydraulic analysis in double-layered microchannels with porous rib and phase change microcapsules slurry as coolant, Int. Commun. Heat Mass Tran. 155 (2024), https://doi.org/10.1016/j.icheatmasstransfer.2024.107489.
[34] B. Li, Y. Cui, G. Li, H. Jiang, Numerical analysis on thermal-hydraulic performance of optimized microchannel heat sink with slant ribs and quatrefoil rib-elliptical groove complex structures, Appl. Therm. Eng. 240 (2024), https://doi.org/10.1016/j.applthermaleng.2023.122165.
[35] H. Sadique, Q. Samsher Murtaza, Numerical Study and Moth Flame optimization of thermal-hydraulic performance of fractal microchannel heat sink with ribs and cavity. https://doi.org/10.2139/ssrn.4822386.
[36] P. Eneren, Y.T. Aksoy, M.R. Vetrano, Experiments on single-phase nanofluid heat transfer mechanisms in microchannel heat sinks: a review, Energies (Basel) 15 (2022), https://doi.org/10.3390/en15072525.
[37] R. Misra, J. Singh, S.K. Jain, S. Faujdar, M. Agrawal, A. Mishra, et al., Prediction of behavior of triangular solar air heater duct using V-down rib with multiple gaps and turbulence promoters as artificial roughness: a CFD analysis, Int. J. Heat Mass Tran. 162 (2020) 120376, https://doi.org/10.1016/j.ijheatmasstransfer.2020.120376.
[38] R. Maithani, J.S. Saini, Heat transfer and friction factor correlations for a solar air heater duct roughened artificially with V-ribs with symmetrical gaps, Exp. Therm. Fluid Sci. 70 (2016) 220–227, https://doi.org/10.1016/j.expthermflusci.2015.09.010.
[39] L. Chai, G. Xia, L. Wang, M. Zhou, Z. Cui, Heat transfer enhancement in microchannel heat sinks with periodic expansion-constriction cross-sections, Int. J. Heat Mass Tran. 62 (2013) 741–751, https://doi.org/10.1016/j.ijheatmasstransfer.2013.03.045.
[40] S. Saha, T. Alam, M.I.H. Siddiqui, M. Kumar, M.A. Ali, N.K. Gupta, et al., Analysis of microchannel heat sink of silicon material with right triangular groove on sidewall of passage, Materials 15 (2022), https://doi.org/10.3390/ma15197020.
[41] K. Derakhshanpour, R. Kamali, M. Eslami, Effect of rib shape and fillet radius on thermal-hydrodynamic performance of microchannel heat sinks: a CFD study, Int. Commun. Heat Mass Tran. 119 (2020), https://doi.org/10.1016/j.icheatmasstransfer.2020.104928.